Article

Secondary Organic Aerosol-Forming Reactions of Glyoxal with Amino Acids

David O. De Haan, Ashley L. Corrigan, Kyle W. Smith, Daniel R. Stroik, Jacob J. Turley, Frances E. Lee, Margaret A. Tolbert, Jose L. Jimenez, Kyle E. Cordova, and Grant R. Ferrell

Environ. Sci. Technol., **2009**, 43 (8), 2818-2824• DOI: 10.1021/es803534f • Publication Date (Web): 12 March 2009

Environ. Sci. Technol. **2009,** *43,* 2818–2824

Secondary Organic Aerosol-Forming Reactions of Glyoxal with Amino Acids

DAVID O. DE HAAN,*,†,‡ ASHLEY L. CORRIGAN,† KYLE W. SMITH,† DANIEL R. STROIK,† JACOB J. TURLEY,† FRANCES E. LEE,† MARGARET A. TOLBERT,‡ JOSE L. JIMENEZ,‡ KYLE E. CORDOVA,‡ AND GRANT R. FERRELL‡

Department of Chemistry and Biochemistry, University of San Diego, 5998 Alcala Park, San Diego California 92110, and Department of Chemistry and Biochemistry, and Cooperative Institute for Research in Environmental Sciences, University of Colorado, Boulder Colorado 80309-0216

Received December 12, 2008. Revised manuscript received February 17, 2009. Accepted February 19, 2009.

Glyoxal, the simplest and most abundant α-dicarbonyl compound in the atmosphere, is scavenged by clouds and aerosol, where it reacts with nucleophiles to form low-volatility products. Here we examine the reactions of glyoxal with five amino acids common in clouds. When glyoxal and glycine, serine, aspartic acid or ornithine are present at concentrations as low as 30 μM in evaporating aqueous droplets or bulk solutions, 1,3-disubstituted imidazoles are formed in irreversible second-order reactions detected by nuclear magnetic resonance (NMR), aerosol mass spectrometry (AMS) and electrospray ionization mass spectrometry (ESI-MS). In contrast, glyoxal reacts with arginine preferentially at side chain amino groups, forming nonaromatic five-membered rings. All reactions were accompanied by browning. The uptake of 45 ppb glyoxal by solid-phase glycine aerosol at 50% RH was also studied and found to cause particle growth and the production of imidazole measured by scanning mobility particle sizing and AMS, respectively, with a glyoxal uptake coefficient $\alpha = 0.0004$. Comparison of reaction kinetics in bulk and in drying droplets shows that conversion of glyoxal dihydrate to monohydrate accelerates the reaction by over 3 orders of magnitude, allowing these reactions to occur at atmospheric conditions.

Introduction

Aerosols have a strong effect on visibility (*1*) and human health (*2*), and can both directly and indirectly influence the climate (*3*). Secondary organic aerosol (SOA) material represents an important fraction of the particle mass throughout the troposphere (*4, 5*). A great amount of effort has been expended to chemically speciate this organic material and understand the processes by which it forms (*6*). Recent comparisons between field measurements and models where both gas-phase aerosol precursor concentrations and aerosol formation rates were measured, however, have shown that our understanding of aerosol formation remains incomplete. In parts of the atmosphere as dissimilar as the Mexico City boundary layer (*7*) and the free troposphere (*8*), SOA formation rates and/or concentrations are much higher than model predictions. The uptake of glyoxal onto aerosol was implicated in Mexico City as being responsible for at least part of the mismatch between measurements and modeling (*9*). Glyoxal is scavenged by aqueous-phase aerosol (*10, 11*) and even by solid aerosol with surface-adsorbed water (*12, 13*).

Cloud processing of small aldehydes, especially glyoxal and methylglyoxal, has also been identified as a source of aerosol (*14*−*16*), supported by field measurements of high levels of oxalic acid, the oxidation product of glyoxal, in the aerosol layer above clouds (*17*). Model runs including glyoxal and methylglyoxal oxidation in clouds and aerosol suggest that these two compounds are responsible for 38% of modeled global SOA, largely via cloud processing (*18*).

The aqueous-phase chemistry of glyoxal is summarized in Scheme 1. Glyoxal takes part in reversible hydration when it enters the condensed phase where it can be oxidized by OH and form oxalic acid. However, at typical atmospheric oxidant concentrations, a large majority of glyoxal is not oxidized within the ∼15 min. lifetime of a cloud droplet (*19*). What then is its fate? ATR-FTIR observations suggest that after most of the water has evaporated from a droplet, the glyoxal dihydrate converts into an extremely reactive monohydrate form, which self-oligomerizes and remains in the condensed phase (*20*). Computations indicate that dehydration may also be triggered by nucleophilic attack (*21*). Amino acids have been implicated in the formation of light-absorbing oligomers via aldol reactions with acetaldehyde (*22, 23*). As we show in this work, the presence of such nucleophiles in an evaporating droplet results in the formation of different nonvolatile products. The resulting dry aerosol then contains these products along with any other low-volatility material from the original droplet, such as oxalic acid.

In this work we describe the reactions between glyoxal and the most common amino acids in clouds, fog, and aerosol (*24*−*26*), and we use electrospray ionization mass spectrometry (ESI-MS) and nuclear magnetic resonance (NMR) to characterize the imidazole products and measure the kinetics of their formation. Finally, we quantify aerosol formation via quadrupole aerosol mass spectrometry (Q-AMS) and high-resolution time-of-flight (HR-ToF)-AMS experiments that simulate cloud droplet drying and the direct uptake of glyoxal by aerosol.

Experimental Methods

^{15}N-enriched glycine (Cambridge Isotopes), amino acids, and glyoxal trimer dihydrate (Sigma-Aldrich) were used without further purification. Glyoxal−amino acid solutions in the concentration range 0.1−1.0 M were made in 18 MΩ water. One μL droplets of these solutions were dried at room temperature on attenuated total reflectance (ATR) 9-reflection diamond crystals (DuraSamplIR, Smiths Detection) and analyzed by Fourier transform infrared (FTIR) spectroscopy (JASCO 4800) in order to observe reactions during the drying process (*20*). Larger 150 μL samples were also dried at room temperature in vials to brown solids, and redissolved in 18 MΩ water at 1 mg/mL for ESI-MS analysis or in D_2O (Cambridge Isotopes) for NMR analysis. Solutions were injected into the ion trap ESI-MS (Thermo-Finnigan LCQ Advantage) via syringe pump at 2.5 μL/min with ESI nozzle voltage = +4.3 kV, medical N_2 sheath gas flow = 25, and

* Corresponding author e-mail: ddehaan@sandiego.edu.
† University of San Diego.
‡ University of Colorado.

10.1021/es803534f CCC: $40.75

Published on Web 03/12/2009

SCHEME 1. Cloud Processing of Glyoxal to Form Imidazole Derivatives, Oligomers, And Oxalic Acid

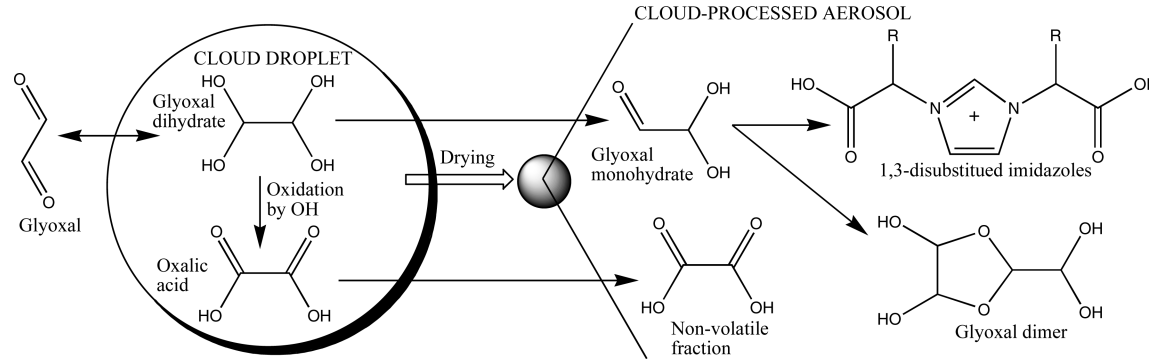

capillary temperature = 200 or 250 °C. ^{1}H, ^{13}C, ^{15}N, and 2-D NMR spectra were collected at room temperature on Varian 400 or 500 MHz instruments. Reaction kinetics were monitored by ^{1}H NMR in D_2O solutions at 295 K containing 1 M glyoxal and either 1 M glycine, 0.86 M arginine, or 0.5 M serine. The latter two amino acids have limited water solubility.

The drying of cloud droplets was simulated by atomizing 0.03−10 mM aqueous mixtures of glyoxal and an amino acid in HPLC-grade water (Sigma-Aldrich) using either pneumatic nebulization (TSI model 9302, 1.5 μm mode wet diameter) or ultrasonic nebulization (~5 μm). The latter was accomplished using an inexpensive, commercially available mist generator that was modified by exposing its conductivity sensor to allow it to work in highly dilute aqueous solutions. Wet drop sizes were calculated from scanning mobility particle sizing (SMPS) distributions for dried NaCl aerosol. The ultrasonically produced mist was pushed by prepurified nitrogen at flow rates of 7−10 L min^{-1} through a charge neutralizer (TSI 3077 or NRD model P-2021−1000) into a collapsible 300 L Teflon chamber (New Star Environmental, LLC) containing nitrogen humidified to >70% RH. Further evaporation from droplets entering the chamber raised the relative humidity beyond 80%, as measured by a humidity sensor (Vaisala HMT337) at the chamber outlet. After ~20 min of fill time, the particles in the chamber were sampled by Q-AMS, (Aerodyne Research) (*27*), HR-ToF-AMS (Aerodyne) (*28*) operating in the highest-resolution "W" mode, or both. Both AMS instruments were operated with vaporizer temperature = 600 °C and 70 eV electron impact ionization. AMS sampling lines were black conductive tubing (TSI) and/or 1/4" o.d. copper and 2−4 m in length. All other aerosol flows were through copper tubing.

Direct uptake of glyoxal by solid-phase glycine aerosol was also probed by Q-AMS and SMPS. A 3 mM glycine solution was ultrasonically nebulized and the droplets were dried to <44% RH, below the efflorescence point (*29*), in the chamber described above. Water vapor was then added to reach 50% RH, staying well below the deliquescence point of 95% RH (*29*). Gas-phase glyoxal was generated by heating equal masses of glyoxal trimer dihydrate and phosphorus pentoxide to 150 °C and trapping the yellow-green gas produced at −105 °C. Glyoxal was purified by trap-to-trap distillation, retaining the middle fraction (*30*). A 1.5 mL flow-through metal vessel was pumped out and pressurized with a few mbar of glyoxal (measured by convection gauge), and the vessel contents were swept into the chamber with dry nitrogen. Glyoxal concentrations in the chamber were calculated to be 45 ppb based on dilution into the current chamber volume. SMPS total aerosol volumes were corrected for volume dilution and for wall losses by fitting the total aerosol volumes before glyoxal addition to a measured first-order decay constant, 0.0034 min^{-1}.

Results and Discussion

Products. Analysis of drops containing 0.1 M glyoxal + glycine by ATR-FTIR shows that the peaks assigned to the amine group at 3174 (asym N—H str), 1508, 1133, and 1188 cm^{-1} (all NH_3^+ deformations) (*31*) are all either eliminated or significantly reduced in intensity upon droplet drying, relative to peaks assigned to glycine's CH_2 or carboxylate group (Figure 1 and Supporting Information Figure S1). In addition, the glyoxal oligomer peaks at 950 and 980 (C—O—C oligomer ring stretch), and 1070 cm^{-1} (C—OH stretch) that appear when glyoxal solutions are dried (*20*) become much less pronounced in the presence of amino acids. These observations suggest that glycine's amine group reacts with glyoxal and largely preempts glyoxal self-reaction.

ESI-MS and NMR data show that glyoxal reacts with the free amino acids glycine, serine, aspartic acid, and ornithine in aqueous solutions to form extremely stable, zwitterionic 1,3-disubstituted imidazoles in irreversible reactions (Scheme 2). ESI-MS spectra of dried and redissolved glyoxal + amino acid bulk solutions are shown in Figure 2 with imidazole peaks labeled. ^{1}H and ^{13}C NMR peak assignments of products formed in glyoxal + amino acid reactions are listed in Supporting Information Table S1. For the reactions of glyoxal with glycine and serine, the imidazoles were the only products detected by ESI-MS or ^{13}C or 2-D NMR experiments. However, the formation of imidazoles was always accompanied by browning of the solution. The compounds causing the brown color are melanoidins, a term used by food chemists to describe complex, light-absorbing, nitrogen-containing oligomer compounds that are end products of Maillard reactions between sugars and amino acids where α-dicarbonyls such as glyoxal are reactive intermediates (*32*). Melanoidins may have been responsible for several small peaks observed by ^{1}H NMR.

Additional products were observed for the reactions of glyoxal with aspartic acid and ornithine. In an ESI mass spectrum (Figure 2), H^+ and Na^+ adducts of unreacted

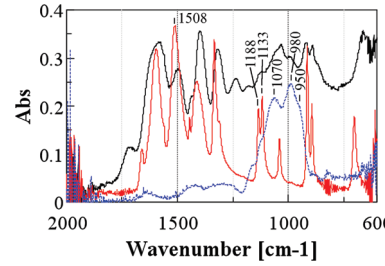

FIGURE 1. Low wavenumber ATR-FTIR peaks observed at the end of drying of aqueous droplets on diamond crystal. Red: 1 uL droplet of 0.095 M glycine. Blue dashed: 5 uL of 0.01 M glyoxal (×2). Black: 1 uL droplet containing 0.095 M glycine and 0.05 M glyoxal.

SCHEME 2. Formation Mechanism for 1,3-Disubstituted Imidazole and Diimine from Glyoxal and the Amino Acids Glycine (*R*═H), Serine (*R*═CH_2OH), Ornithine (*R*═$CH_2CH_2CH_2NH_2$), and Aspartic Acid (*R*═CH_2COO^-); Odd Carbon Designated by *

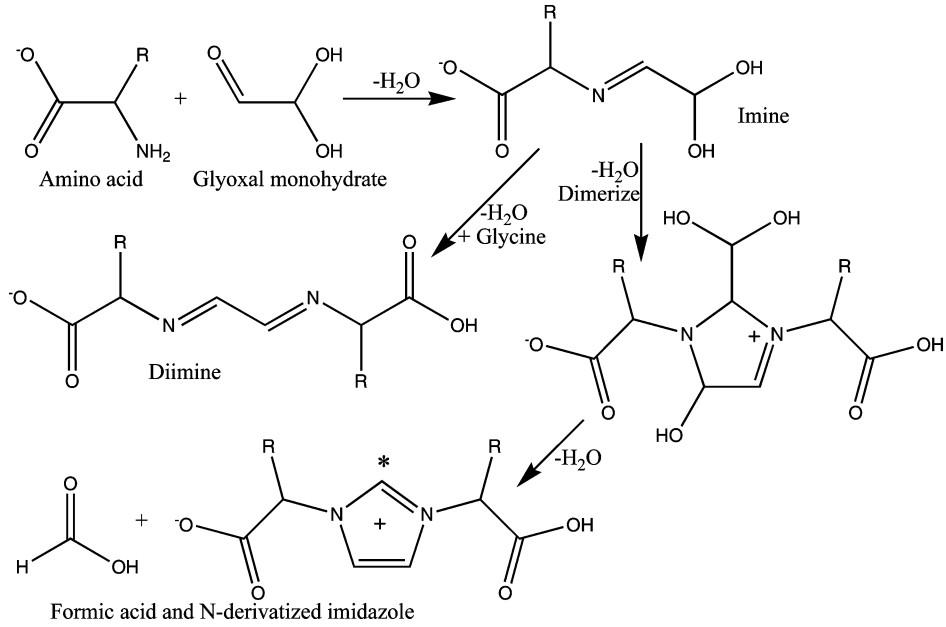

aspartic acid are dominant at m/z 134 and 156, and the imidazole peak at m/z 301 is only one of several significant product peaks. While the glyoxal−ornithine imidazole peak at m/z 299 is dominant in ESI-MS (Figure 2), multiple isomers are observed by NMR because of ornithine's two reactive amine groups. Integration of ^{1}H NMR data suggests that glyoxal reacts at ornithine's α-amine group 80% of the time, and only 20% of the time at the side chain amine group. The reaction with glyoxal requires a deprotonated amino group.

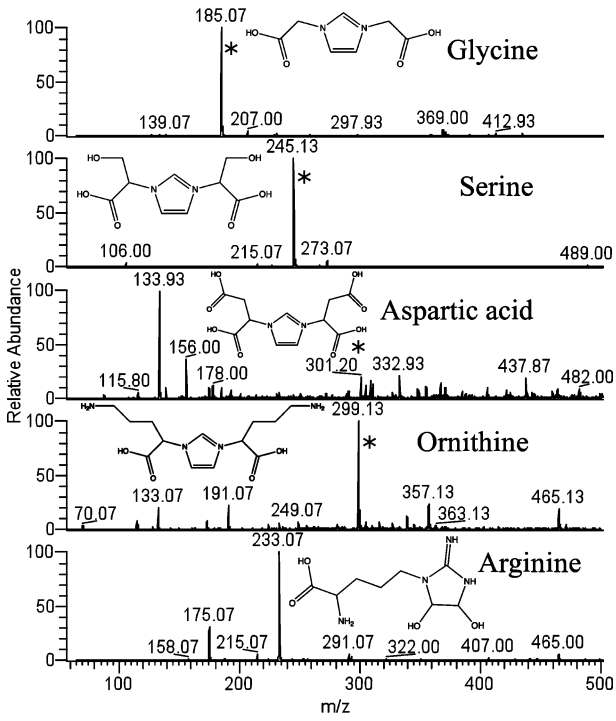

FIGURE 2. Electrospray ionization mass spectra of the products of bulk phase reactions of glyoxal with amine compounds, after drying to a solid residue and redissolving residue in water to reach 1 mg/mL. Absolute abundances (all × 10^6): Glycine, 2.7 Serine, 16.1. Aspartic acid, 0.88. Ornithine, 4.0. Arginine, 14.5. * denotes mass of 1,3-disubstituted imidazole product shown.

The preference for the α-amine position is likely due to its higher probability of deprotonation; its pK_a is 8.69 compared to 10.76 for the side chain amine group.

The irreversible formation of 1,3-disubstituted imidazoles has been previously observed for the room temperature reaction of glyoxal and glycine (*33*), the reaction between glyoxal, formaldehyde, and several amino acids at 80 °C (*34*), and the reaction of glyoxal with lysine side chains, which causes protein cross-linking under physiological conditions (*35*). The imidazole yield is highest under mildly acidic conditions (pH 3−5); however, melanoidin formation (brown discoloration) was maximized at pH 8 for nonacidic amino acids and pH 5 for glutamic acid (*34*). We hypothesize that imidazole formation in the absence of formaldehyde begins with a nucleophilic attack by an unprotonated amine group on glyoxal monohydrate's carbonyl moiety (Scheme 2). Proton transfer followed by water loss produces an imine intermediate. Reaction at glyoxal's second carbonyl (after dehydration) produces a diimine, a minor product to which we assign the 8.1 ppm ^{1}H NMR peak (Supporting Information Table S1) based on other diimines characterized by Nielsen et al. (*36*). In 1 M glyoxal + glycine experiments, imines react with each other 80% of the time (based on relative ^{1}H NMR signals for the products), forming a zwitterion intermediate, which cyclizes and gains an H^+ to form the five-membered ring (*36*). Dehydration then triggers the C—C bond rupture and loss of formic acid, forming the disubstituted imidazole with an "odd carbon" not bonded to another carbon (marked with * in Scheme 2). Several lines of evidence in support of this mechanism are presented below.

Previous workers have attributed the odd carbon in the imidazole ring to the addition of formaldehyde produced in the Strecker degradation of glycine (*33*). This mechanism would leave a third amino acid side chain *R* attached to the odd carbon of the imidazole ring. While the product is the same regardless of the source of the odd carbon atom for the reaction with glycine (*R*═H), other amino acids will produce different products. Since products masses containing a third *R* group were not observed (Figure 2) for serine (m/z 275), aspartic acid (m/z 359), or ornithine (m/z 356), we conclude that the odd carbon in all our experiments must be from a second glyoxal molecule.

TABLE 1. Room-Temperature ^{1}H-NMR Kinetics Data for the Reactions of Glyoxal with Amino Acids (AA) in D_2O in the Absence of Drying

amino acid	[glyoxal] (M)	[AA] (M)	$f_{glyoxal}$[a]	f_{AA}	AA initial loss rate (mM d^{-1})	2nd order rate constant, k[b] (M^{-1} s^{-1})
glycine	1.0	1.0	7×10^{-4}	1.7×10^{-4}[c]	1.9 ± 0.6	0.12 ± 0.04
serine	1.0	0.48	7×10^{-4}	7.1×10^{-4}[c]	2.0 ± 0.2	0.09 ± 0.01
arginine	1.0	0.86	7×10^{-4}	1	24 ± 3	$(4.5 \pm 0.6) \times 10^{-4}$

[a] Fraction of glyoxal in monohydrate form estimated using thermodynamic parameters from *ab initio* computations (*21*). [b] Expressed in terms of concentrations of reactive forms of glyoxal and amino acids. [c] Fraction of amino acid with deprotonated amine group at pH 6.

SCHEME 3. Products Formed in Glyoxal + Arginine Reaction

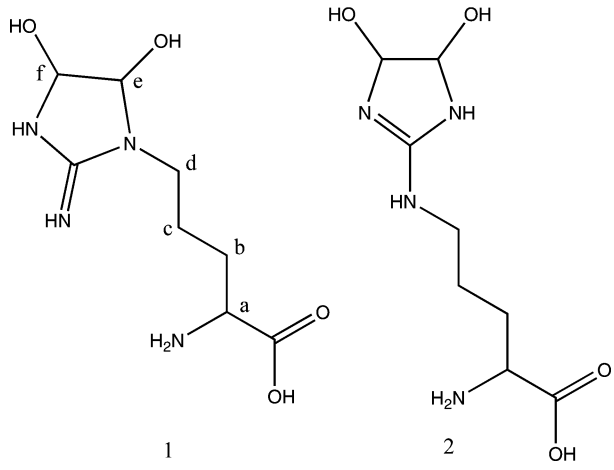

1 2

Similar quantities of *N*-derivatized imidazoles were produced even if bulk glyoxal + amino acid mixtures were dried in the dark or under nitrogen. While it is unusual for C—C bonds to rupture without photolysis or oxidant chemistry, the very high thermodynamic stability of the aromatic imidazole ring is pivotal. We do not believe that the imidazole peaks observed by ESI-MS are the result of fragmentation because NMR data clearly indicates a hydrogen atom attached at the odd carbon. Furthermore, there is no NMR evidence for either an attached aldehyde or *gem*-diol group that would be expected if the second glyoxal carbon atom were still attached to the imidazole ring.

The reaction between glyoxal and arginine is different from those of the other amino acids because arginine's side chain contains three amine groups, two of which can react even when one is protonated. Thus, glyoxal reacts twice at the arginine side chain, forming 1:1 adducts rather than imidazoles. The major products **1** and **2** (Scheme 3), both with protonated m/z 233 (Figure 2), were identified by NMR and were produced in a ratio of 3:1. Products from the reaction of glyoxal at the arginine α-amine group are at least 30 times less abundant. The imidazolidine derivative of **1**, produced by a single dehydration followed by hydride transfer (*37*), is observed when glyoxal is incubated at 110 °C with proteins (*38*).

Kinetics. Figure 3 and Supporting Information Figures S2 and S3 show the time dependence of the peak areas of ^{1}H NMR peaks assigned to amino acids, diimine and imidazole products (Supporting Information Table S1) for the reactions between glyoxal and arginine, serine, and glycine. A graph of 1/[reactant] vs time (Supporting Information Figure S2) is most linear for a second order reaction with reactants present in equimolar quantities, and this was observed for all three reactions. Because glyoxal−amino acid reactions must occur between glyoxal monohydrate and amino acids with unprotonated amine groups, we express the rate law as

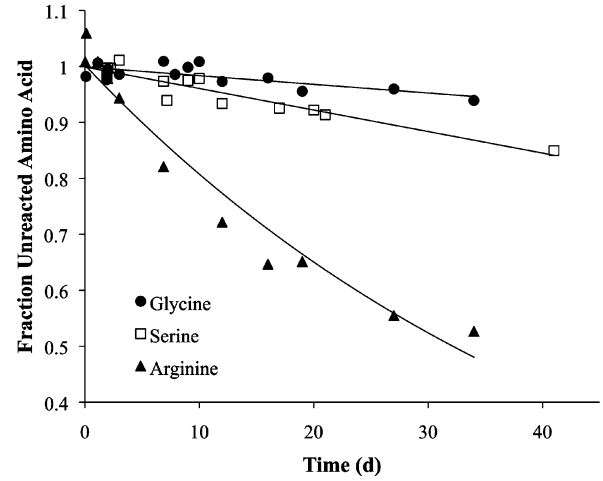

FIGURE 3. Kinetics of amino acid loss during reactions with glyoxal at room temperature in D_2O, without drying. Two reactions per amino acid were performed; all data is shown together. Amino acids are quantified by relative peak areas of major ^{1}H NMR signals, normalized to 1 at t = 0. Initial concentrations: glyoxal and glycine = 1.0 M, serine = 0.48 M, and arginine = 0.86 M. Reaction rates are calculated from initial loss rates, taken to be a linear fit to all data for glycine and serine (as shown) and to first 7 days of data for arginine (linear fit not shown). Curve shown for arginine is to guide the eye.

$$\frac{-d[\mathrm{AA}]}{dt} = k_{\mathrm{AA}}[\mathrm{Glyoxal}]_{\mathrm{tot}} f_{\mathrm{glyoxal}} [\mathrm{AA}]_{\mathrm{tot}} f_{\mathrm{AA}} \quad (1)$$

where AA is any amino acid, k_{AA} is the rate constant in M^{-1} s^{-1} expressed in terms of the reactive forms of each reactant, $[\mathrm{Glyoxal}]_{tot}$ and $[\mathrm{AA}]_{tot}$ are the concentrations of all forms of the reactants in M in the aqueous phase, and f is the fraction of each reactant in reactive form:

$$f_{\mathrm{glyoxal}} = \frac{[\mathrm{GlyoxalMonohydrate}]}{[\mathrm{Glyoxal}]_{\mathrm{tot}}} \quad (2)$$

$$f_{\mathrm{AA}} = \frac{[\mathrm{NH_2CHRCOO^-}]}{[\mathrm{AA}]_{\mathrm{tot}}} \quad (3)$$

These fractions were estimated using the results of ab initio calculations for glyoxal (*21*), pK_a values for the amino acids glycine and serine, and experimental pH 6. Since $[\mathrm{Glyoxal}]_{tot} \approx [\mathrm{GlyoxalDihydrate}]$ in solution, $f_{glyoxal}$ represents an equilibrium constant for the dehydration reaction of glyoxal dihydrate. Because the arginine side chain appears to be reactive even when protonated, all arginine molecules are considered to be active-form reactants, $f_{Arg} = 1$. Rate constants were then calculated in terms of these fractions and measured initial reaction rates (Table 1). Glyoxal loss rates were not measured, but should be the same as the amino acid loss rates listed.

Time-dependent yields of diimine and imidazole products (produced in glycine and serine systems) remained proportional throughout each experiment (Supporting Information Figure S3), suggesting that diimines are side-products rather than intermediates, consistent with Scheme 1. Imine signals were not observed, consistent with a short-lived intermediate whose formation is rate-determining.

Reaction stoichiometry and yields can be estimated by comparing growth rates of NMR product peaks with the amino acid loss rates. For the reaction between glyoxal and glycine, the production rate of the imidazole product (measured at the 7.4 ppm peak due to two CH groups on the ring) is 60 ± 20% of the loss rate for glycine (measured at the CH_2 group peak at 3.4 ppm and propagating 1σ uncertainties in the slopes). Because each of the signals is due to 2 H atoms, the rates are directly comparable, and suggest that ~1.2 ± 0.4 imidazole product molecules form for each two glycine molecules that react. Similarly, the production rate for the diimine intermediate (measured at the 8.1 ppm peak due to two CH imine groups) is 15 ± 5% of the glycine loss rate, indicating that 0.3 ± 0.1 diimine product molecules are formed per two glycine reactants. The total observed product formation stoichiometry is 1.5 ± 0.5 molecules per two glycine, within uncertainty of the expected stoichiometry of 1:2, and suggesting that no other products were formed in significant amounts. A similar analysis of the reaction with arginine confirms net stiochiometric yields for products **1** and **2** (Supporting Information Table S1).

Concentration Dependence and Cloud Droplet Drying. We simulated the drying of cloud droplets by generating aqueous ~5 μm droplets containing 4 mM glycine and glyoxal (but no inorganic salts) and introducing them into a chamber at 90% RH. When the resulting aerosol was sampled 10 min later by HR-ToF-AMS, 1,3-disubstituted imidazole product was observed at m/z 185, along with larger fragment peaks such as m/z 86, $C_3H_4NO_2^+$. The relative abundances of these peaks changed only slightly with further sampling or drying, suggesting that the reaction was nearly complete by the first sampling. When the experiment was repeated at atmospherically relevant reactant concentrations of 32 μM (125 times less concentrated), the molecular ion peak was no longer visible, but the m/z 86 fragment was still detectable with an abundance 2000 times lower. Other product fragment ions observed by both Q-AMS and HR-ToF-AMS (containing both C and N, m/z 97, $C_4H_3NO_2^+$ and m/z 126, $C_5H_6N_2O_2^+$), responded proportionally to changes in reactant concentrations, suggesting that the glycine−glyoxal reaction has an overall reaction order of ~1.6, roughly consistent with NMR kinetics results described above.

The AMS results provide direct evidence that imidazole formation can occur on a time scale of minutes in an evaporating droplet that contains atmospheric concentrations of glyoxal and amino acid (2−200 μM (*39, 41*) and 1−100 μM (*24, 25*), respectively). If we assume that the drying process in our experiment results in aerosol with water/glycine/glyoxal present at a 5:1:1 molar ratio at 90% RH (consistent with electrodynamic balance measurements for water and glycine (*29*)), solute concentrations would be ~5 M. Using the active form fractions f and rate constant listed in Table 1, we would predict that the reaction would take months unless we include the drying-induced conversion of glyoxal dihydrate to its reactive monohydrate form. With $f_{glyoxal} = 1$, predicted reaction times are within a factor of 6 of the ~30 min reaction times observed by the AMS, but still too slow. The remaining difference is likely due to enhanced deprotonation of the glycine amine group in the mixed organic/water aerosol phase making $f_{glycine} > 1.7 \times 10^{-4}$. Thus, the rapidity of the observed reaction in drying droplets relative to bulk solutions is further evidence that drying converts both reactants to active forms by the time the water mole fraction declines to 0.7, but to different extents.

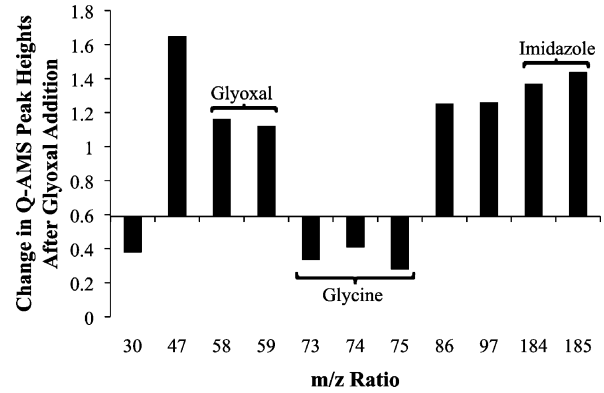

FIGURE 4. Q-AMS peak height changes for peaks exhibiting the largest relative change upon exposure of solid glycine aerosol at 50% RH to 45 ppb gas-phase glyoxal. Changes are expressed as ratios of average signals postexposure divided by pre-exposure. The total AMS aerosol-phase signal declined by 41% due to wall losses. All bars are referenced to this benchmark, so that any peaks that declined by more than this are shown as negative, whereas peaks that increased in size extend above 1. HR-ToF-AMS peak identifications are shown in figure. Other peaks: *m/z* 30 (CH_4N^+ glycine fragment), 47 (formic acid or $H_3CO_2^+$ fragment), 86 (product fragment $C_3H_4NO_2^+$), 97 (product fragment $C_4H_3NO_2^+$). Full Q-AMS spectra are shown in Supporting Information Figure S4.

Glyoxal Uptake by Aerosol. Since reactions between glyoxal and amino acids accelerate during droplet evaporation, they may occur at the highest rates in aerosol particles (*13*). We examined this process by exposing solid-phase glycine aerosol (mode diameter = 84 nm) at 50% RH to 45 ppb of gas-phase glyoxal, while analyzing the resultant aerosol by SMPS and Q-AMS. (All fragment identifications were confirmed by HR-ToF-AMS in drying droplet studies.) Total aerosol volume at the time of glyoxal addition was 1.2×10^3 $\mu m^3\ cm^{-3}$, which means that glyoxal and glycine were present in equimolar quantities in the chamber. The addition of glyoxal triggered 30 min. of particle growth, increasing aerosol volume by 20% (after wall loss and volume dilution corrections) and increasing particle-phase glyoxal signals at m/z 58 (Figure 4 and Supporting Information Figure S4). Furthermore, significant signal increases occurred at m/z 184 and 185 (imidazole product), 86 and 97 (major product fragments), and 47 ($H_3CO_2^+$), which is either formic acid produced in Scheme 1, or more likely an ionization fragment of larger aerosol-phase molecules. Glyoxal addition also caused glycine Q-AMS peaks at m/z 30 and 73−75 to decline by half (after normalizing for the general decline in total aerosol-phase signal) (Figure 4 and Supporting Information Figure S4). If half of the glycine reacts to form imidazole product via a 1:1 reaction with glyoxal, if byproduct water and formic acid evaporate in the AMS inlet as expected, and if the density of the 1,3-disubstituted imidazole product is the same as that of imidazole (1.03 g/cm^3), then the expected volume growth would be 19%, matching our SMPS aerosol growth observation.

These observations suggest that glyoxal uptake onto solid amino acid aerosol is a reactive process and not simply a function of the interaction of glyoxal with aerosol water content. The cessation of particle growth after 30 min is likely caused byproduct buildup at the solid aerosol surface, which physically separates the reactants. An uptake coefficient for glyoxal on solid-phase glycine, defined as the fraction of molecular collisions with the aerosol surface that result in glyoxal uptake, can be estimated (*12*) based on this experiment to be $\alpha = 4 \times 10^{-4}$. This is about an order of magnitude

less than the uptake coefficient inferred for glyoxal on Mexico City aerosol (*9*).

Atmospheric Significance. If a 5 μm cloud droplet contained 30 μM of both glyoxal and amino acids, and a complete conversion to imidazole product ensued, the amount of resulting imidazole product would make up at least 2% by volume of a typical cloud processed aerosol with diameter = 130 nm. Thus, we can estimate that the reactants glyoxal and amino acids in an evaporating cloud droplet would be diluted by about a factor of 50 by other nonvolatile compounds compared to our simulated cloud droplet drying experiments. Under these circumstances, using aerosol-phase reactant concentrations of 5 M/50 = 0.1 M, $f_{\text{glyoxal}} = 1$ and $f_{\text{glycine}} = 6 \times 1.7 \times 10^{-4}$, and the rate constant for the glyoxal + glycine reaction, conversion to 1,3-disubstituted imidazoles would take ~1 day, much less than the average atmospheric lifetime of aerosol particles. The temperature dependence of glyoxal−amino acid reactions is unknown, however.

Glyoxal concentrations range from 10 to 40 ppt over most of the earth's surface, with enhanced levels observed over tropical, oceanic, and urban regions (*42*). Amino acids are often enriched in marine precipitation by a factor of 10 over terrestrial precipitation (*24*), and by ~3 orders of magnitude over surface seawater (*43*). Measured organic N/C atomic ratios have ranged from ~0.02 in Mexico City aerosol (*44*) to ~0.2 in Central Valley fog (*45*). Imidazole and melanoidin formation from glyoxal−amino acid reactions likely occurs over vast regions of the ocean, over rainforests, and in "hot spots" where urban plumes mix with biologically derived aerosol.

Acknowledgments

This material is based upon work supported by the National Science Foundation under Grant No. ATM-0749145 and by Research Corporation for Science Advancement. We thank Michael Cubison and Donna Sueper for assistance with HR-ToF-AMS hardware and software and Brandon Connelly for synthesizing gas-phase glyoxal.

Note Added after ASAP Publication

Two references were added to the version published on March 12, 2009. The corrected version was published on March 20, 2009.

Supporting Information Available

NMR peak assignments, ATR-FTIR data, NMR kinetics data, and Q-AMS spectra before and after glyoxal uptake by glycine aerosol. This material is available free of charge via the Internet at http://pubs.acs.org.

Literature Cited

(1) Watson, J. G. Visibility: science and regulation. *J. Air Waste Manage. Assoc.* **2002**, *52*, 628–713.
(2) Harrison, R. M.; Yin, J. Particulate matter in the atmosphere: which particle properties are important for its effects on health. *Sci. Total Environ.* **2000**, *249*, 85–101.
(3) Kanakidou, M.; et al. Organic aerosol and global climate modelling: A review. *Atmos. Chem. Phys.* **2005**, *5*, 1053–1123.
(4) Zhang, Q.; et al. Ubiquity and dominance of oxygenated species in organic aerosols in anthropogenically-influenced Northern Hemisphere midlatitudes. *Geophys. Res. Lett.* **2007**, *34*, L13801/1–6.
(5) Murphy, D. M.; et al. Single-particle mass spectrometry of tropospheric aerosol particles *J. Geophys. Res* **2006**, *111*, D23S32, DOI: 10.1029/2006JD007340.
(6) Hallquist, M.; et al. The formation, properties and impact of secondary organic aerosol: current and emerging issues. *Atmos. Chem. Phys. Discuss.* **2009**, *9*, 3555–3762.
(7) Volkamer, R.; et al. Secondary organic aerosol formation from anthropogenic air pollution: Rapid and higher than expected *Geophys. Res. Lett.* **2006**, *33*, L17811, DOI: 10.1029/2006GL026899.
(8) Heald, C. L.; et al. A large organic aerosol source in the free troposphere missing from current models. *Geophys. Res. Lett.* **2005**, *32*, L18809.
(9) Volkamer, R.; et al. A missing sink for gas-phase glyoxal in Mexico City: formation of secondary organic aerosol. *Geophys. Res. Lett.* **2007**, *34*, L19807.
(10) Liggio, J.; Li, S.-M.; McLaren, R. Reactive uptake of glyoxal by particulate matter. *J. Geophys. Res.* **2005**, *110*, D10304.
(11) Kroll, J. H.; et al. Chamber studies of secondary organic aerosol growth by reactive uptake of simple carbonyl compounds *J. Geophys. Res* **2005**, *110*, D23207, DOI: 10.1029/2005JD006004.
(12) Hastings, W. P.; et al. Secondary organic aerosol formation by glyoxal hydration and oligomer formation: humidity effects and equilibrium shifts during analysis. *Environ. Sci. Technol.* **2005**, *39*, 8728–8735.
(13) Corrigan, A. L.; Hanley, S. W.; De Haan, D. O. Uptake of glyoxal by organic and inorganic aerosol. *Environ. Sci. Technol.* **2008**, *42*, 4428–4433.
(14) Lim, H.-J.; Carlton, A. G.; Turpin, B. J. Isoprene forms secondary organic aerosol through cloud processing: Model simulations. *Environ. Sci. Technol.* **2005**, *39*, 4441–4446.
(15) Altieri, K. E.; et al. Evidence for oligomer formation in clouds: reactions of isoprene oxidation products. *Environ. Sci. Technol.* **2006**, *40*, 4956–4960.
(16) Ervens, B.; et al. Secondary organic aerosol yields from cloud-processing of isoprene oxidation products. *Geophys. Res. Lett.* **2008**, *35*, L02816.
(17) Sorooshian, A.; et al. On the source of organic acid aerosol layers above clouds. *Environ. Sci. Technol.* **2007**, *41*, 4647–4654.
(18) Fu, T.-M.; et al. Global budgets of atmospheric glyoxal and methylglyoxal, and implications for formation of secondary organic aerosols. *J. Geophys. Res.* **2008**, *113*, D15303.
(19) Ervens, B.; et al. A modeling study of aqueous production of dicarboxylic acids: 1. Chemical pathways and speciated organic mass production. *J. Geophys. Res.* **2004**, *109*, D15205.
(20) Loeffler, K. W.; et al. Oligomer formation in evaporating aqueous glyoxal and methyl glyoxal solutions. *Environ. Sci. Technol.* **2006**, *40*, 6318–6323.
(21) Kua, J.; Hanley, S. W.; De Haan, D. O. Thermodynamics and kinetics of glyoxal dimer formation: a computational study. *J. Phys. Chem. A* **2008**, *112*, 66–72.
(22) Nozière, B.; Dziedzic, P.; Córdova, A. Formation of secondary light-abosrbing "fulvic-like" oligomers: a common process in aqueous and ionic atmospheric particles? *Geophys. Res. Lett.* **2007**, *34*, L21812.
(23) Nozière, B.; Córdova, A. A kinetic and mechanistic study of the amino acid catalyzed aldol condensation of acetaldehyde in aqueous and salt solutions. *J. Phys. Chem. A* **2008**, *112*, 2827–2837.
(24) Mopper, K.; Zika, R. G. Free amino acids in marine rains: evidence for oxidation and potential role in nitrogen cycling. *Nature* **1987**, *325*, 246–249.
(25) Zhang, Q.; Anastasio, C. Free and combined amino compounds in atmospheric fine particles ($PM_{2.5}$) and fog waters from Northern California. *Atmos. Environ.* **2003**, *37*, 2247–2258.
(26) Matsumoto, K.; Uematsu, M. Free amino acids in marine aerosols over the western North Pacific Ocean. *Atmos. Environ.* **2005**, *39*, 2163–2170.
(27) Canagaratna, M. R.; et al. Chemical and microphysical characterization of ambient aerosols with the Aerodyne aerosol mass spectrometer. *Mass Spectrom. Rev.* **2007**, *26*, 185–222.
(28) DeCarlo, P. F.; et al. Field-deployable, high-resolution, time-of-flight aerosol mass spectrometer. *Anal. Chem.* **2006**, *78*, 8281–8289.
(29) Chan, M. N.; et al. Hygroscopicity of water-soluble organic compounds in atmospheric aerosols: amino acids and biomass derived organic species. *Environ. Sci. Technol.* **2005**, *39*, 1555–1562.
(30) Volkamer, R.; Ziemann, P. J.; Molina, M. J. Secondary organic aerosol formation from acetylene (C_2H_2): seed effect on SOA yields due to organic photochemistry in the aerosol aqueous phase. *Atmos. Chem. Phys. Discuss.* **2008**, *8*, 14841–14892.
(31) Fischer, G.; et al. The FT-IR spectra of glycine and glycineglycine zwitterions isolated in alkali halide matrices. *Chem. Phys.* **2005**, *313*, 39–49.
(32) Cammerer, B.; Jalyschko, W.; Kroh, L. W. Intact carbohydrate structures as part of the melanoidin skeleton. *J. Ag. Food Chem.* **2002**, *50*, 2083–2087.
(33) Velisek, J.; et al. New imidazoles formed in nonenzymatic browning reactions. *J. Food Sci.* **1989**, *54*, 1544–1546.
(34) Davidek, T.; et al. Amino acids derived 1,3-disubstituted imidazoles in nonenzymatic browning reactions. *Sb. Vys. Sk.*

Chem.-Technol. Praze, E: Potraviny **1991**, *62*, 165–182.
(35) Chellan, P.; Nagaraj, R. H. Protein crosslinking by the Maillard reaction: dicarbonyl-derived imidazolium crosslinks in aging and diabetes. *Arch. Biochem. Biophys.* **1999**, *368*, 98–104.
(36) Nielsen, A. T.; et al. Polyazapolycyclics by condensation of aldehydes with amines. 2. Formation of 2,4,6,8,10,12-hexabenzyl-2,4,6,8,10,12-hexaazatetracyclo [5.5.0.0^{5,9}.0^{3,11}]dodecanes from glyoxal and benzylamines. *J. Org. Chem.* **1990**, *55*, 1459–1466.
(37) Chassonery, D.; et al. Reactions de dismutation a partir du glyoxal et de molecules basiques difonctionnelles. *Bull. Soc. Chim. Fr.* **1994**, *131*, 188–199.
(38) Schwarzenbolz, U.; et al. On the reaction of glyoxal with proteins. *Z. Lebensm. Unters. Forsch. A* **1997**, *205*, 121–124.
(39) Igawa, M.; Munger, J. W.; Hoffmann, M. R. Analysis of aldehydes in cloud- and fogwater samples by HPLC with a postcolumn reaction detector. *Environ. Sci. Technol.* **1989**, *23*, 556–561.
(40) Munger, J. W.; et al. Formaldehyde, glyoxal, and methylglyoxal in air and cloudwater at a rural mountain site in central Virginia. *J. Geophys. Res.* **1995**, *100*, 9325–9333.
(41) Matsumoto, K.; Kawai, S.; Igawa, M. Dominant factors controlling concentrations of aldehydes in rain, fog, dew water, and in the gas phase. *Atmos. Environ.* **2005**, *39*, 7321–7329.
(42) Wittrock, F.; et al. Simultaneous global observations of glyoxal and formaldehyde from space. *Geophys. Res. Lett.* **2006**, *33*, L16804.
(43) Milne, P. J.; Zika, R. G. Amino acid nitrogen in atmospheric aerosols: occurrence, sources and photochemical modification. *J. Atmos. Chem.* **1993**, *16*, 361–398.
(44) Aiken, A. C.; et al. O/C and OM/OC ratios of primary, secondary, and ambient organic aerosols with high-resolution time-of-flight aerosol mass spectrometry. *Environ. Sci. Technol.* **2008**, *42*, 4478–4485.
(45) Zhang, Q.; Anastasio, C. Chemistry of fog waters in California's Central Valley-Part 3: Concentrations and speciation of organic and inorganic nitrogen. *Atmos. Environ.* **2001**, *35*, 5629–5643.

ES803534F

Secondary organic aerosol-forming reactions of glyoxal with amino acids

Supplemental Information

David O. De Haan,[1,2] Ashley L. Corrigan,[1] Kyle W. Smith,[1] Daniel R. Stroik,[1] Jacob J. Turley,[1] Frances E. Lee,[1] Margaret A. Tolbert,[2] Jose L. Jimenez,[2] Kyle E. Cordova,[2] Grant R. Ferrell[2]*

Contents: 6 pp total

Table S1: ^{1}H- and ^{13}C-NMR peak assignments for the major (left side) and minor (right side) products of the reactions of glyoxal with amino acids.

Product Structures:	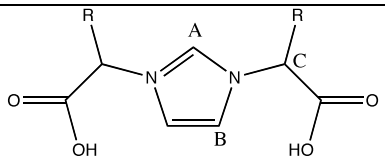 N-derivatized imidazole							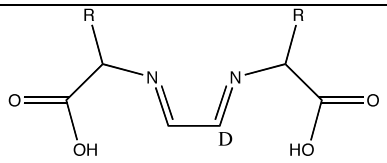 Diimine	
		A	B	C	R-group			D	
Glycine	^{1}H	8.6	7.3	4.6	na			8.1	
	^{13}C	137	123	52	na				
Serine	^{1}H	8.8	7.4	4.0	4.1			8.2	
Ornithine	^{1}H	8.7	7.4	4.1	1.8	1.6	2.9	8.0	
	^{13}C	136	123	63	25	23	39		
Aspartic acid	^{1}H	8.97 [a]	7.4	5.28	2.5			8.3	
	^{13}C	138.0 [a]	123.4 [a]	62.4 [a]	39.0 [a]				
Product Structures:	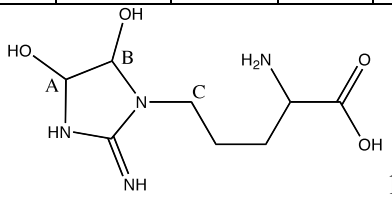 1							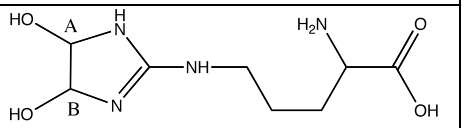 2	
		A	B	C	R			A	B
Arginine	^{1}H	5.0	5.0	3.3	1.7	1.8	3.6	5.2	5.2
	^{13}C	83	89	41	24	28	54	77	83

a: NMR data from Davidek, et al.,(32) synthesized including formaldehyde.

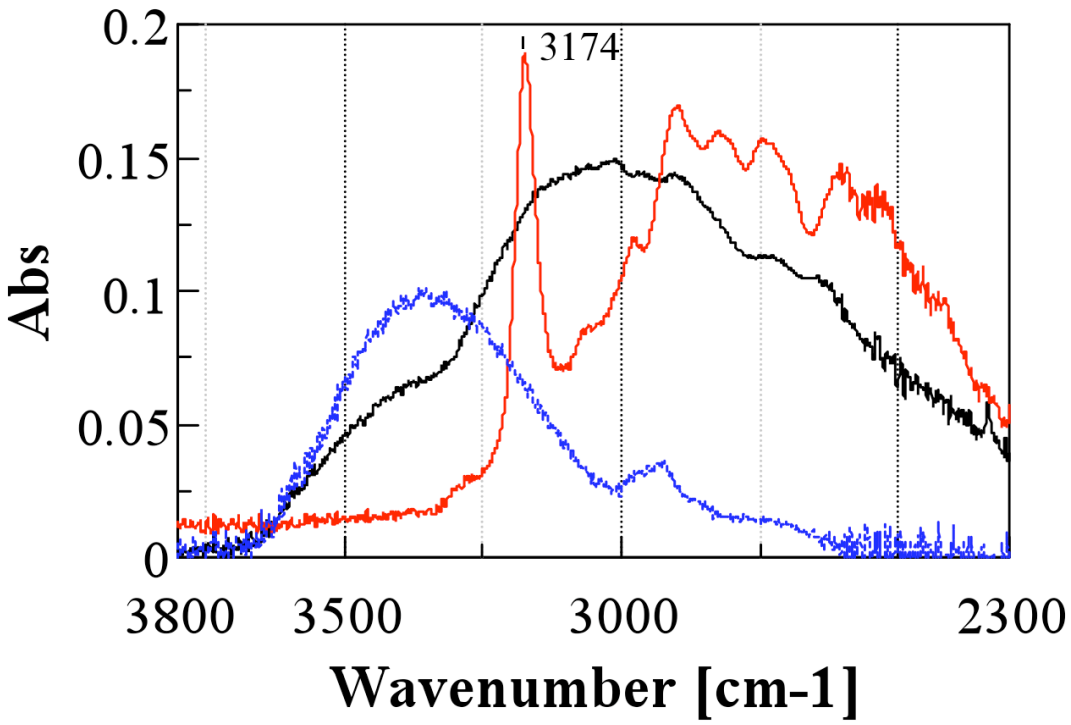

Figure S1: High wavenumber ATR-FTIR peaks observed at the end of drying of aqueous droplets on diamond crystal. Red: 1 uL droplet of 0.095 M glycine. Blue dashed: 5 uL of 0.01 M glyoxal (× 2). Black: 1 uL droplet containing 0.095 M glycine and 0.05 M glyoxal.

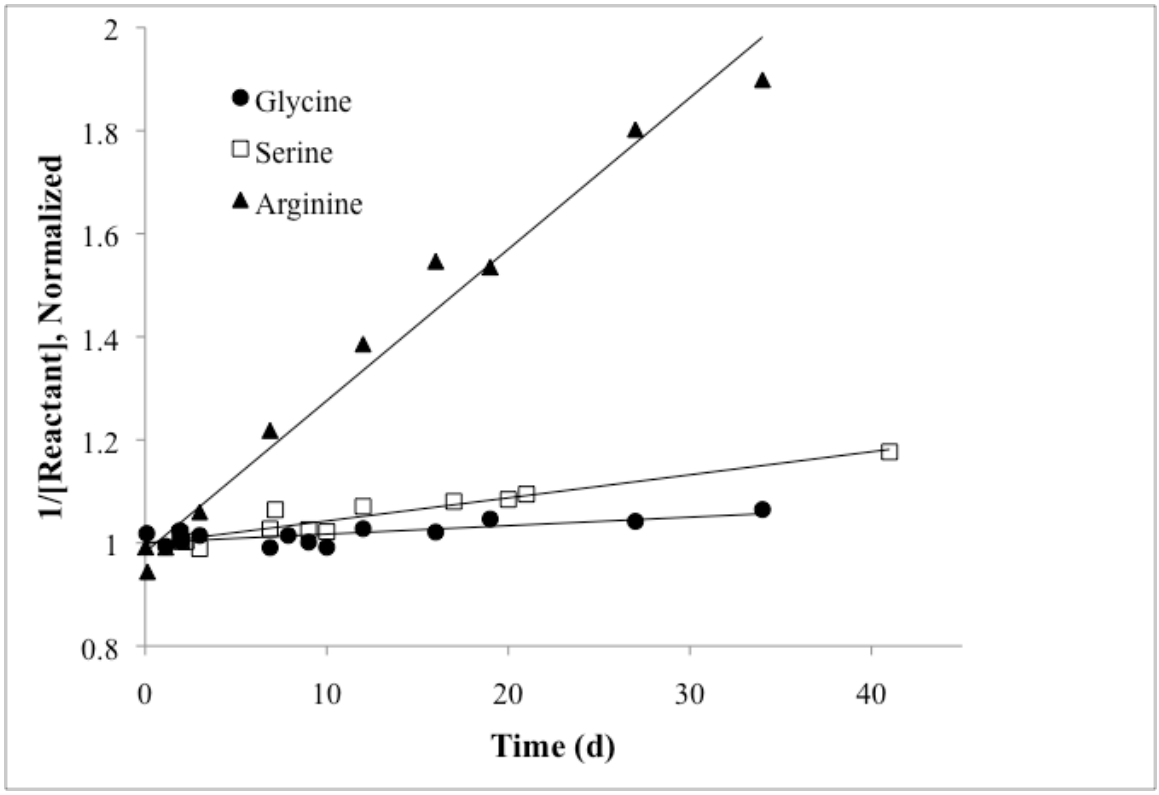

Figure S2: Kinetics data from Figure 3, graphed as $\frac{1}{[AA]}$ vs time, where *AA* is the normalized amino acid concentration. Data is for glyoxal + amino acid reactions performed at room temperature in D_2O, without drying. Initial concentrations: glyoxal and glycine = 1.0 M, serine = 0.48 M, and arginine = 0.86 M. Two reactions per amino acid were performed; all data is shown.

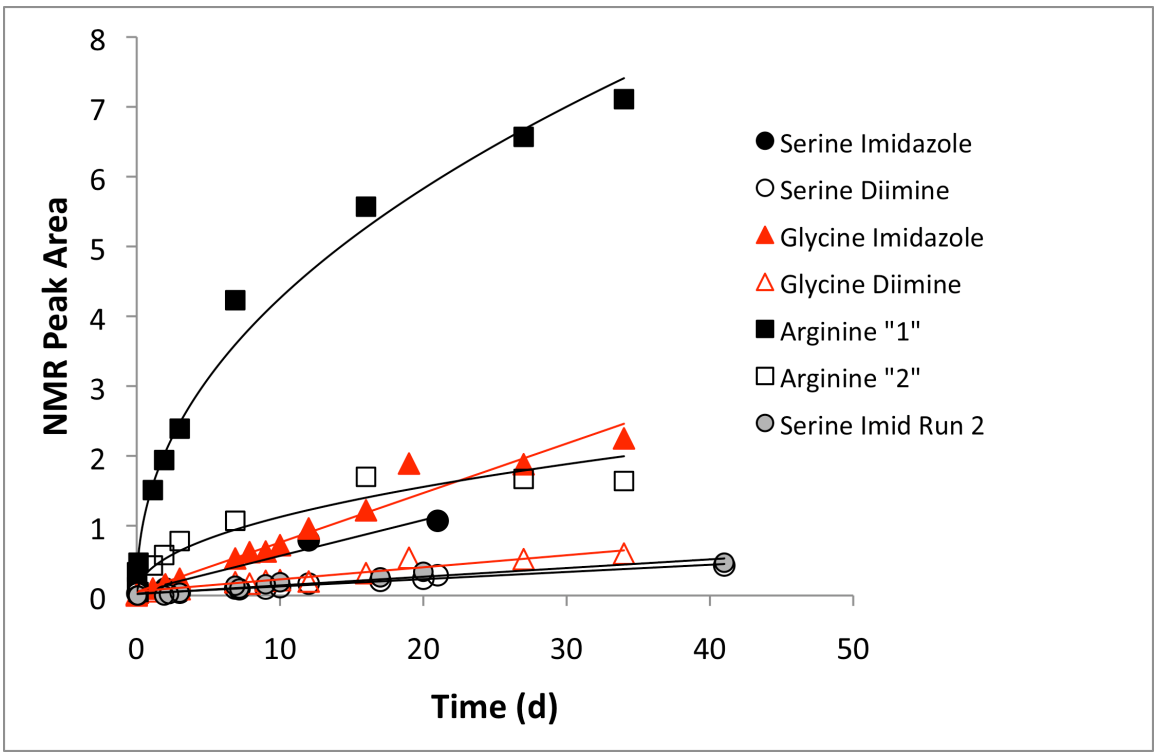

Figure S3: Kinetics of product appearance during glyoxal + amino acid reactions shown in Fig. S2. Imidazole production from glyoxal + serine was inconsistent, so the two runs are shown separately. Products are quantified by relative peak areas of major ^{1}H-NMR signals. Lines shown are guides for the eye.

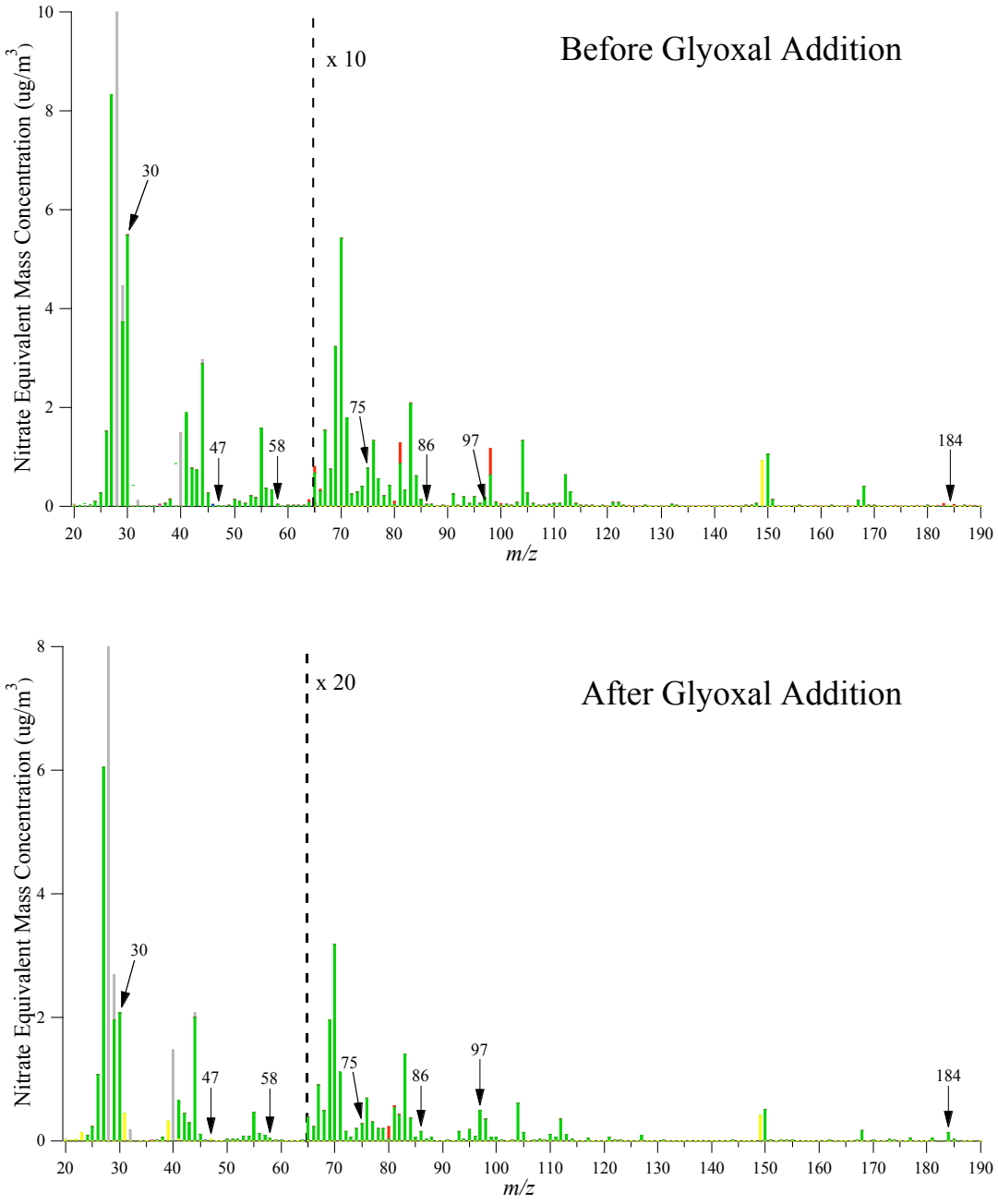

Figure S4: Comparison of averaged Q-AMS stick spectra collected for solid glycine aerosol at 50% RH before and after exposure to 45 ppb gas-phase glyoxal. The aerosol signal declined overall by 41% between the two sets of spectra, so the data in the bottom panel is expanded vertically for easier comparison. Peaks discussed in the text are labeled. AMS color code: Organic: green. Air: gray. Sulphate: red. Other: yellow.